MTLA 45 (2026) 102636

Contents lists available at ScienceDirect

Materialia

journal homepage: www.elsevier.com/locate/mtla

Magnetic behaviour of FeCo-2V under applied stress and elevated temperature

Sirapob Toyting [a,*], Christopher W. Harrison [b], Alexis Lambourne [c], Howard J. Stone [a]

[a] University of Cambridge, Department of Materials Science and Metallurgy, 27 Charles Babbage Road, Cambridge CB3 0FS, UK
[b] Cardiff University, School of Engineering, Cardiff CF24 3AA, UK
[c] Rolls-Royce Plc, PO Box 2000, Derbyshire, DE24 7XX, UK

ARTICLE INFO

Keywords:
FeCo-2V alloy
Soft magnet
Coercivity
Core losses
Magnetostriction
Resistivity

ABSTRACT

FeCo-2V alloys are promising candidates for high-performance electric machines, such as those used in aerospace and electrification, owing to their exceptional saturation magnetisation and potential to maximise power density. Nevertheless, their magnetic behaviour under mechanical loading and at elevated temperatures remains insufficiently understood. In this study, the stress- and temperature-dependent magnetic and electrical properties of FeCo-2V were investigated separately, with particular attention to coercivity, core losses, and underlying mechanisms. Stress-dependent experiments revealed three distinct regimes. Under compressive loading, magnetic performance deteriorated, as shown by expanding hysteresis loops and increased coercivity and core losses due to hard-axis magnetisation. In the tensile regime below ~100 MPa, performance improved through stress-assisted easy-axis alignment. At higher tensile stresses, however, micro-yielding dominated: increasing Kernel Average Misorientation (KAM) angles indicated enhanced dislocation densities, which in turn degraded magnetic properties. Independent temperature-dependent studies demonstrated that coercivity decreases systematically with increasing temperature, attributed to reduced anisotropy energy that facilitates domain wall motion. Core losses also declined with temperature, with loss-separation analysis confirming reductions in both hysteresis and eddy current loss coefficients. Additionally, electrical resistivity was observed to increase with temperature, consistent with the Drude model and a reduced eddy current loss coefficient.

1. Introduction

Soft magnetic materials are critical in a range of applications including power generation, magnetic shielding, and data storage due to their high permeability and low coercivity [1–4]. Among these materials, iron-cobalt (FeCo) alloys stand out for their exceptional magnetic properties, including high Curie temperatures, superior saturation magnetisation, excellent permeability, and low core losses, alongside acceptable mechanical strength and remarkable corrosion resistance [3–7]. These characteristics make FeCo alloys the preferred material for applications requiring power dense or torque dense magnetic components, such as generators and motors for aerospace electrification. However, their comparatively high cost restricts their use to niche applications where their performance justifies the expense.

A key composition in FeCo soft magnetic materials is the FeCo-2V alloy, discovered in 1932, which offers improved ductility and workability [7,8], making it more attractive for industrial applications requiring both mechanical reliability and high magnetic performance [6,7]. Despite its advantages, the behaviour of FeCo-2V under mechanical stress, critical for engineering applications, remains insufficiently understood. Previous studies have demonstrated that stress significantly alters magnetic properties, with tensile stresses generally reducing coercivity and improving permeability, while compressive stresses have the opposite effect [9,10]. To better contextualise these effects, prior work on soft magnetic materials provides valuable insights. For example, Lahyaoui et al. [11] studied the magnetic properties of non-oriented Si-Fe steels under compressive and tensile stress and found that compression induces magnetic hardening, while tension improves permeability. Similarly, Iordache and Hug [10] observed similar compression-induced hardening in Si-Fe steels and FeCo-2V, suggesting a broader trend across soft magnetic alloys. Miyagi et al. [12] reported comparable stress-dependent magnetic degradation in electrical steels, reinforcing the significance of stress-microstructure interactions. Interestingly, Gorkunov et al. [13] demonstrated that even tensile stress

* Corresponding author.
E-mail address: st788@cam.ac.uk (S. Toyting).

https://doi.org/10.1016/j.mtla.2025.102636
Received 25 September 2025; Accepted 13 December 2025
Available online 13 December 2025

could degrade magnetic properties in 09G2S pipe steel, highlighting material-specific responses. In contrast, Turgut et al. [9] investigated FeCo alloys and found that moderate tensile stress reduces coercivity and power losses, aligning with Iordache and Hug's [10] observations in FeCo-2V. Despite these advances, the underlying mechanisms linking stress, microstructure, and magnetostriction in FeCo-2V remain unresolved. This knowledge gap limits the effective utilisation of FeCo-2V alloys in stress-prone environments.

Another underexplored area concerns the thermal behaviour of FeCo-2V. Understanding its performance at elevated temperatures is critical for real-world applications, where thermal effects can significantly affect magnetic behaviour. This hinders its utilisation in high-temperature environments, where thermal effects can significantly impact magnetic performance. The lack of data also reduces the accuracy of electrical machine models, thereby limiting effective sizing and optimisation of the associated cooling systems.

Over the past few decades, existing research has extensively investigated the thermal-dependent behaviour of various soft magnetic alloys. For example, Ferraris et al. [14] investigated the temperature dependence of coercivity and core losses in Soft Magnetic Composite (SMC) materials. They observed a reduction in both properties as temperature increased from 20 °C to 125 °C, attributing this to thermal energy aiding domain wall motion and reducing pinning effects. Similarly, Groh et al. [15] reported a decrease in coercivity in FeCo alloys at elevated temperatures, linking this phenomenon to grain growth and a reduction in domain wall pinning at grain boundaries. Li et al. [16] also demonstrated a reduction in hysteresis losses in ferritic materials under similar conditions, further supporting the general trend of improved magnetic properties with increasing temperature. While these studies provide valuable insights into the thermal behaviour of soft magnetic materials, studies have predominantly focussed on composites and FeSi alloys, leaving a gap in understanding the specific response of FeCo-2V to temperature variations.

To address these gaps, this study investigates the stress-dependent and temperature-dependent magnetic behaviour of FeCo-2V in two separate but complementary parts. The magnetic properties under applied stress or temperature were determined using a Single Sheet Tester (SST) at a range of frequencies that enabled loss separation analysis. The microstructural changes associated with applied stress were determined with Electron Backscatter Diffraction (EBSD) with Kernel Average Misorientation (KAM) analysis. The effect of temperature on resistivity was also characterised to elucidate the origins of thermal degradation or improvement of magnetic performance. The results aim to provide insights into FeCo-2V behaviour under practical operating conditions and to inform the design of high-performance electrical machines where both mechanical and thermal reliability are essential.

2. Material and methods

2.1. Sample preparation and heat treatment

Sheets of Vacoflux 50 and Vacodur 49 were obtained from Vacuumschmelze. Vacoflux 50 has a nominal composition of 49 wt.% Fe, 49 wt.% Co, and 2 wt.% V, while Vacodur 49 contains the same base composition with a small addition of niobium. The sheets were supplied in the cold-rolled state with thicknesses of 0.2 mm. This thickness was selected as it is typical of that used in industrial electric motor applications.

In this study, two closely related FeCo–2V–based alloys were used for different experimental campaigns. Vacoflux 50 was used for all stress-dependent magnetic property measurements and the EBSD/KAM microstructural analyses, while Vacodur 49 was used for the temperature-dependent magnetic property measurements and resistivity experiments.

The only compositional distinction between the two alloys is the small niobium addition in Vacodur 49 (typically <0.3 wt.% Nb). Nb additions are known to influence grain growth behaviour in Fe–Co–V alloys. Prior work by Shang et al. [17] demonstrated that Nb-containing alloys exhibit slower grain growth during annealing because Nb-rich precipitates reduce grain-boundary mobility. This grain-refining effect stabilises the microstructure but does not alter the fundamental stress- or temperature-dependent magnetic mechanisms discussed in this study. Therefore, while Vacodur 49 may experience slightly slower grain coarsening than Nb-free Vacoflux 50, the underlying magneto-mechanical and magneto-thermal responses remain fully comparable between the two alloys.

Prior to heat treatment, the Vacoflux 50 and Vacodur 49 strip samples were cleaned with acetone to remove any surface contaminants that could affect the heat treatment results. The heat treatment was done according to standard commercialised practice to achieve a 'mechanical anneal' [18]. This heat treatment was carried out in controlled atmosphere of dry, pure hydrogen gas to prevent oxidation. The samples were heated to a target temperature of 750 °C at a controlled rate of 15 °C/min and held isothermally for 3 hours to ensure uniform recrystallisation and stress relief [19,20]. After the isothermal hold, the samples were cooled slowly in the same hydrogen atmosphere at a rate of 100–300 °C/hour until they reached ambient temperature. Following the final heat treatment, the microstructure of the stress-free FeCo-2V samples was characterised using SEM to establish a baseline condition. The recrystallised grains exhibited an average grain size of approximately 10 μm. The grain size distribution was moderately broad but centred around this value.

2.2. In situ stress magnetic properties measurement

The magnetic properties of the Vacoflux 50 FeCo-2V samples were measured using a Single Sheet Tester (SST). The SST operates by applying an alternating magnetic field to the sample via a coil, inducing magnetic flux within the material that generates eddy currents and hysteresis losses. By analysing the induced voltage and current in the coil, the coercivity and core loss of the sample can be accurately quantified [21,22].

For this study, the FeCo-2V samples were tested under both compressive and tensile stresses using Brockhaus Measurements' SST system, which complies with the IEC 60404-3 standard [23]. Stress levels ranged from -50 MPa (compressive) to 300 MPa (tensile) and were applied along the sample's length, parallel with the applied magnetic field. To assess frequency-dependent behaviour and enable loss separation analysis, measurements were conducted at four frequencies: 50, 400, 1000, and 1600 Hz.

2.3. EBSD – Kernel Average Misorientation (KAM)

The effect of mechanical stress on microstructure was evaluated via EBSD analysis of samples subjected to applied tensile stresses of 100, 200, and 300 MPa.

Prior to scanning, surface preparation involved grinding with 600, 1200, and 2500 grit SiC papers, followed by polishing using diamond paste (6 μm, 3 μm, 1 μm, and 0.25 μm) and colloidal silica suspensions. An oil-based lubricant was used during polishing to prevent oxidation.

Mapping was carried out using a Zeiss Gemini SEM 300 equipped with an Oxford Instruments Symmetry detector. Data were collected using Aztec software under 20 kV accelerating voltage, with a 60 μm aperture, 0.5 μm pixel size, and 4 ms dwell time, maintaining a 17.5 mm working distance. The sample stage was tilted at 70° to capture the diffraction pattern. Each scan covered a 500 μm × 500 μm area. Kernel Average Misorientation (KAM) values were extracted using MTEX in MATLAB to assess the extent of plastic deformation at different stress levels.

2.4. Magnetic properties testing under elevated temperature

In-situ magnetic properties testing over a range of temperatures was conducted using a Single Sheet Tester (SST) machine. The AC magnetisation of Epstein samples (300 mm × 30 mm thin Vacodur 49 magnetic sheets) was controlled using a National Instruments LabVIEW program, which employed a feedback loop to generate a standard B-waveform in accordance with IEC 60404-4 [24,25]. The system included a National Instruments DAQ PCI-6120, an EP4000 Europower 4000 W power amplifier, an isolation transformer, and a 0.49 Ω shunt resistor [26]. The desired waveform was generated by the DAQ device, amplified, and passed through the isolation transformer to eliminate DC offsets. The voltage across the shunt resistor was used to determine the coil current, and thus the magnetic field strength (H-field), while feedback from the sense coil was used to calculate the sample's B-field (flux density). To minimise the influence of air flux, sense coils were wound directly onto the sample. Magnetic properties such as power loss and permeability were then calculated by the program based on the recorded hysteresis loop [21,22]. A thermocouple was attached to the sample to precisely record its temperature. The temperature was varied from 24 °C to 150 °C, with measurements taken every 10 °C. To facilitate loss separation analysis, measurements were made at six distinct frequencies: 60 Hz, 100 Hz, 300 Hz, 400 Hz, 600 Hz and 800 Hz.

2.5. Loss – separation analysis

To quantify individual loss mechanisms in the both *in situ* stress and elevated temperature experiments, the total magnetic energy loss (P_{total}) was separated into three components: hysteresis loss (P_h), eddy current loss (P_{ed}), and excess loss (P_{ex}), as expressed by:

$$P_{total} = P_h + P_{ex} + P_{ed} \quad (1)$$

These losses were described using the Bertotti model [27], which relates them to frequency (f) and magnetic flux density (B):

$$P_{total} = k_h B^n f + k_{ex} B^{3/2} f^{3/2} + k_{ed} B^2 f^2 \quad (2)$$

The constants k_h, k_{ex} and k_{ed} correspond to hysteresis, excess, and eddy current losses, respectively. The Steinmetz exponent n is a material-dependent value typically falling between 1.5 and 2 for soft magnetic materials [1].

The model was transformed by dividing both sides by frequency:

$$\frac{P_{total}}{f} = k_h B^n + k_{ex} B^{3/2} f^{1/2} + k_{ed} B^2 f \quad (3)$$

This expression simplified the curve-fitting process, allowing more accurate determination of each loss component [28,29].

2.6. Resistivity measurement

Resistivity measurements were conducted by the National Physical Laboratory using the four-point contact method, in compliance with the BS EN 60404-13:1996 standard [30]. FeCo-2V samples with dimensions of 300 mm × 30 mm × 0.1 mm were used for the measurements. In this method, two brass connectors, serving as the outer probes, were placed in contact with either end of each strip sample to apply a measured current of approximately 0.5 A. Simultaneously, knife edges, acting as the inner probes with a nominal separation of 200 mm, were positioned in contact with the sample to measure the resulting voltage drop. This configuration ensures that the voltage measurement is unaffected by contact resistance at the electrodes, as the inner probes do not carry current.

The measurement setup was positioned at the centre of a temperature-controlled chamber, and measurements were conducted over a temperature range of -40 °C to 170 °C. The temperature variation during each measurement was maintained within ± 0.1 °C. At each temperature, the system was allowed to thermally equilibrate before measurements were taken, ensuring accurate and consistent results.

The resistance obtained from these measurements was used to calculate the material's resistivity using Eq. 4:

$$\rho = \frac{Rbd}{l} \quad (4)$$

where ρ is the resistivity, R is the measured resistance, b is the sample width, d is the strip thickness and l is the electrical path length or distance between two inner probes. Resistivity measurements were recorded at 10 °C intervals across the specified temperature range and repeated for three separate FeCo-2V strips to ensure reproducibility and accuracy.

3. Results

3.1. Magnetic hysteresis behaviour under applied compressive stress

The application of compressive stresses generated significant changes in the hysteresis characteristics of FeCo-2V (Fig. 1a). At 0 MPa, the material exhibited hysteresis loops with minimal area, indicating relatively low energy loss during the magnetisation cycle. When compressive stress increased to -10 MPa and -50 MPa, two changes were observed: (1) the loops underwent clockwise rotation, (2) their width and the overall loop area increased. These modifications suggest a stress-induced transition in magnetisation mechanisms. The loop expansion correlates directly with increasing coercivity, demonstrating the stress sensitivity of magnetic hardening in this alloy system.

3.2. Magnetic hysteresis behaviour under applied tensile stress

In contrast to compressive loading, applied tensile stress induced different hysteresis behaviour (Fig. 1b and 1c). The most striking difference appeared in loop shape, with samples developing progressively more 'square' loops as the tensile stress increased compared to the linear shaped loops at zero and compressive stresses. This shape difference indicates fundamentally different domain dynamics under the two stress states. At moderate tensile stresses (<100 MPa), the loops contracted and coercivity decreased (Fig. 1b). However, beyond the critical ~ 100 MPa threshold, the loops began expanding horizontally, with coercivity increasing (Fig. 1c). This non-monotonic response implies competing mechanisms: initial stress-enhanced domain alignment followed by stress-induced defect generation at higher loads.

3.3. Stress dependence of coercivity and core losses

Coercivity is presented as a function of applied stress in Fig. 2a. Under compressive stress, the value of coercivity rises with the increase in compressive stress. In contrast, within the range of tensile stress from 0 MPa to approximately 100 MPa, coercivity decreases as the tensile stress increases. Beyond around 100 MPa, a further increase in tensile stress leads to a slight increase in coercivity.

Core loss measurements (Fig. 2b) revealed similar stress dependence as coercivity. Under compression, total losses increased for all tested frequencies compared to the stress-free state. The tensile regime showed the characteristic two-stage behaviour: a reduction in total losses below 100 MPa followed by an increase above this threshold.

3.4. Loss-separation analysis of in situ stress data

Loss-separation analysis was implemented to investigate the rise in core loss in the tensile stress range of 100 MPa to 300 MPa. In this work, the eddy current loss term was excluded from Eq. 3 during the loss separation process. This assumption was based on the fact that eddy current loss is largely governed by material conductivity, sample

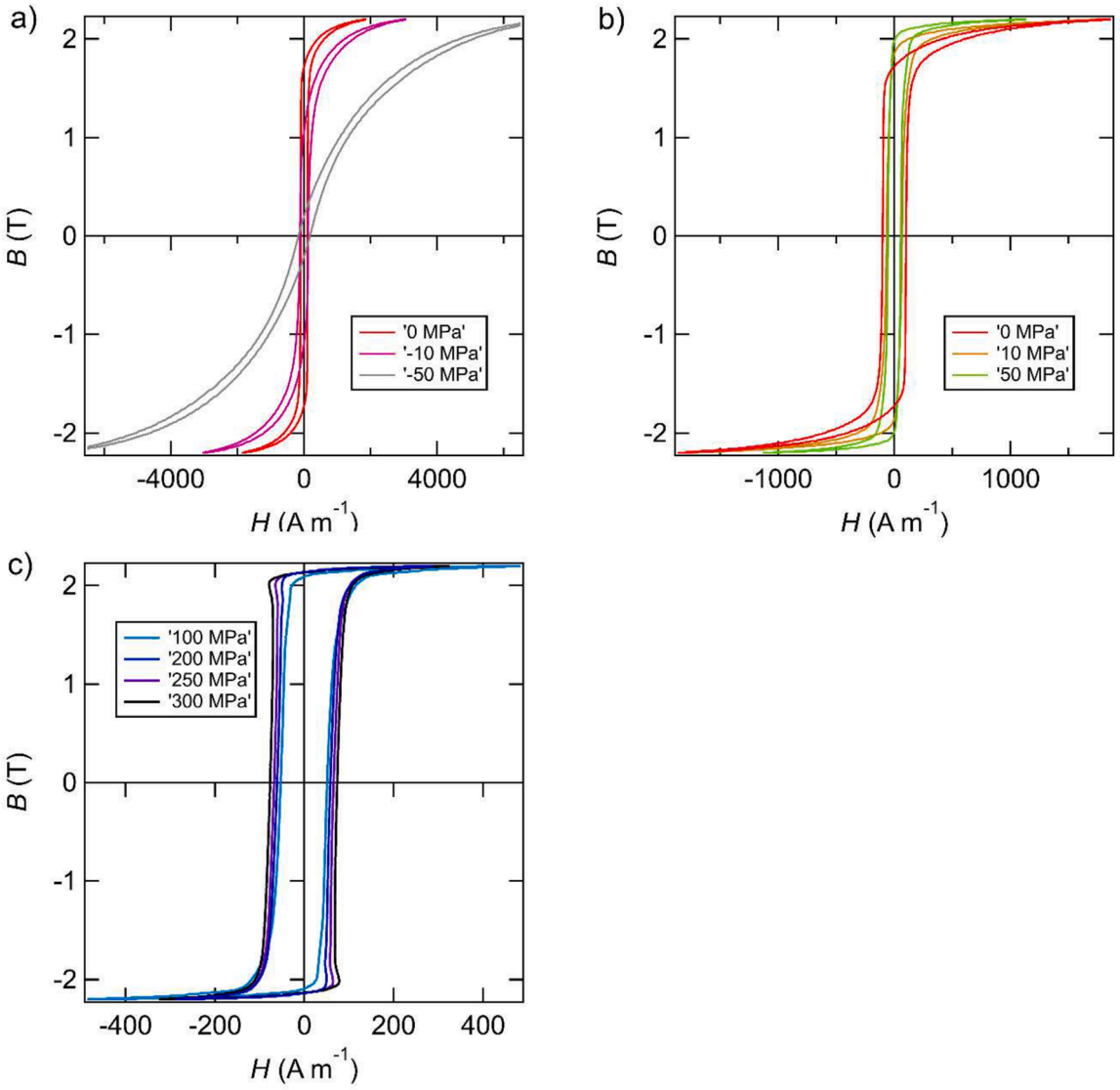

Fig. 1. Hysteresis loops of FeCo-2V a) under compressive stresses of -50 MPa to 0 MPa and under tensile stresses of b) 0 MPa to 50 MPa and c) 100 MPa to 300 MPa (frequency = 50 Hz).

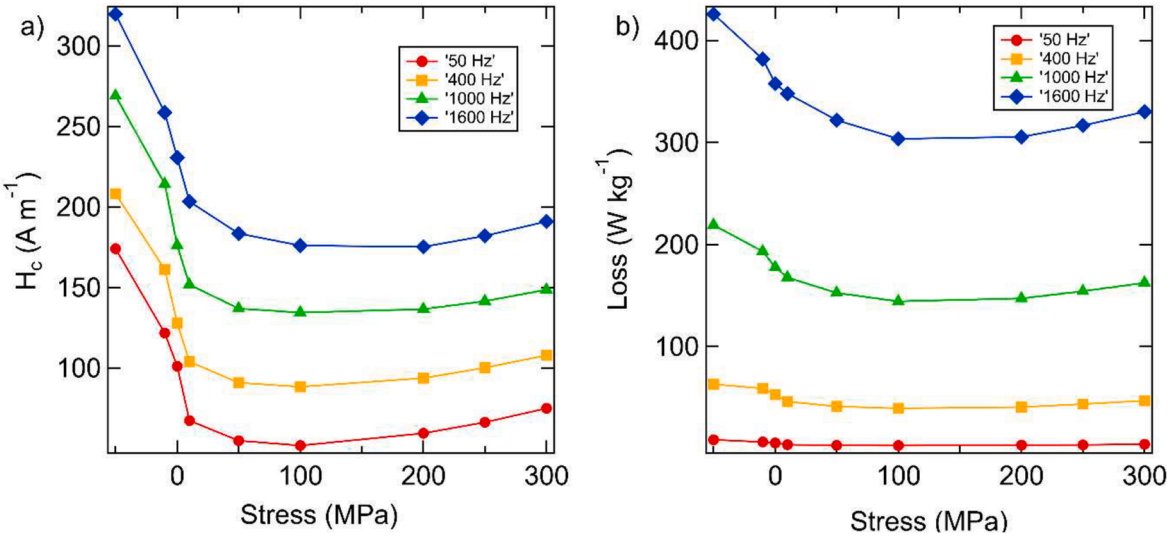

Fig. 2. a) a plot of coercivity of FeCo-2V against applied stress and b) plot of core loss of FeCo-2V against applied stress.

geometry, and the frequency of the applied magnetic field [27,31]. Given that all FeCo-2V specimens were obtained from the same production batch and possessed comparable thicknesses, differences in eddy current loss among the samples were deemed negligible.

To justify the omission of the eddy current term, the relative magnitude of each loss component was estimated at the frequencies used in this study. Using the fitted eddy current coefficient k_{ed} obtained from elevated-temperature measurements, the eddy current loss was calculated from

$$P_{ed} = k_{ed}B^2f^2 \tag{5}$$

at $B = 2$ T and $f = 50$ Hz, representative of the lowest frequency used in the stress experiments. At this condition, P_{ed} contributes less than 10 % of the measured total loss.

Importantly, the variation in eddy current loss between samples subjected to different stresses is negligible, as all samples have identical thickness, conductivity, and geometry.

Furthermore, the excess loss slopes in Fig. 3 are nearly identical across all stress levels, indicating that excess loss does not change with applied stress.

As a result, the stress-dependent changes in total loss originate from the hysteresis component, justifying the use of the simplified loss-separation expression (Eq. 6) for analysing the effect of stress on magnetic losses.

$$\frac{P_{total}}{f} = k_hB^n + k_{ex}B^{3/2}f^{1/2} \tag{6}$$

Eq. 6 was then used to construct plots of $\frac{P_{total}}{f}$ against $f^{1/2}$, yielding a linear trend. In this representation, the y-intercept corresponds to k_hB^n, while the slope represents $k_{ex}B^{3/2}$.

Fig. 3 shows the loss separation plot of $\frac{P_{total}}{f}$ against $f^{1/2}$ for four samples subjected to different tensile stresses (100, 200, 250 and 300 MPa). The selection of data presented was based on the measurements made under a magnetic flux density (B) equal to 2 T. Based on Eq. 6, the data were plotted, and straight lines were fitted for all data. The y-intercept and gradient of the fitted line are labelled in the text box as a and b, respectively. All straight lines show similar slopes, indicating that their excess loss coefficients (k_{ex}) are almost the same among these four samples. Therefore, the rise in core loss is dominated by hysteresis loss.

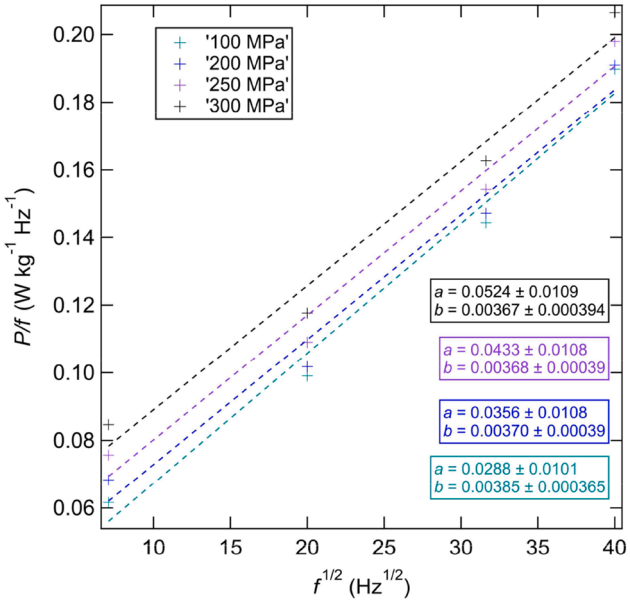

Fig. 3. Loss separation analysis plot of FeCo-2V samples deformed at different tensile stresses.

The calculated hysteresis loss coefficients (k_h), determined from the y-intercept values, exhibited distinct stress dependence (Fig. 4). As tensile stress increased from 100 MPa to 300 MPa, the k_h coefficient showed a progressive rise. This increasing trend aligned with the increase in total core losses throughout the tested stress range.

3.5. EBSD – Kernel Average Misorientation (KAM)

Electron backscatter diffraction (EBSD) was used to examine FeCo-2V samples subjected to tensile stresses of 100, 200, and 300 MPa. The MTEX toolbox was used to process the EBSD data to generate KAM maps, with the resulting misorientation angle distributions presented as violin plots in Fig. 5. These plots show the full distribution of misorientation angles, where red markers indicate mean values, and black contours represent the distribution of misorientations across each sample.

The analysis revealed that increasing tensile stress led to broader distributions of misorientation angles, reflecting greater microstructural heterogeneity. Samples subjected to higher deformation levels showed both increased average misorientation angles and more frequent occurrences of high-angle misorientations. Quantitatively, the mean misorientation angles rose progressively from 0.43° after 100 MPa to 0.51° after 200 MPa and 0.54° after 300 MPa. This consistent increase indicates a direct relationship between applied stress and the development of local distortions in the material.

3.6. Magnetic properties measurement at elevated temperature

The magnetic properties of the FeCo-2V alloy, measured over a range of temperatures, are presented in the form of hysteresis loops, coercivity and core loss measurements. Example hysteresis curves measured at 24 °C, 70 °C and 110 °C are shown in Fig. 6a. All hysteresis curves were similar in shape but differed in area. The hysteresis loop measured at 24 °C, presented in red, had the largest area while the hysteresis loop measured at 110 °C, shown in blue, had the smallest area. This indicates that energy dissipation was highest in the sample measured at 24 °C and lowest in the sample measured at 110 °C.

A comparison of coercivity values measured at 100 Hz is shown in Fig. 6b. Coercivity, identified as the intersection of the hysteresis loop with the x-axis, was found to decrease with increasing temperature. The sample measured at 110 °C exhibited the lowest coercivity (105.87 A m^{-1}), while the sample measured at 24 °C showed the highest coercivity

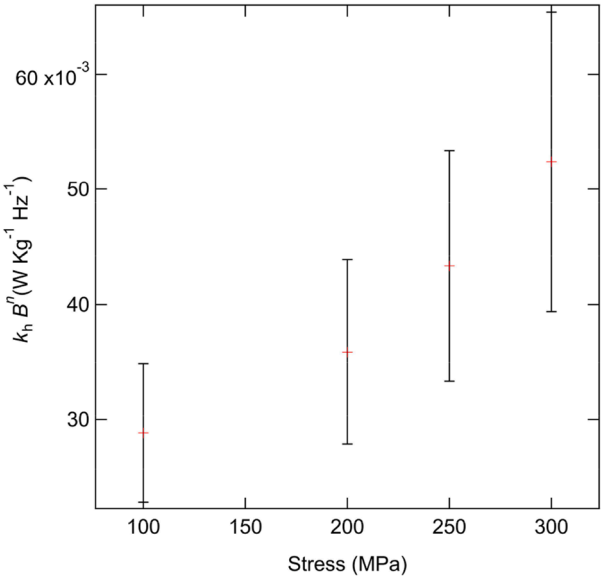

Fig. 4. A plot of hysteresis loss coefficient against applied tensile stress.

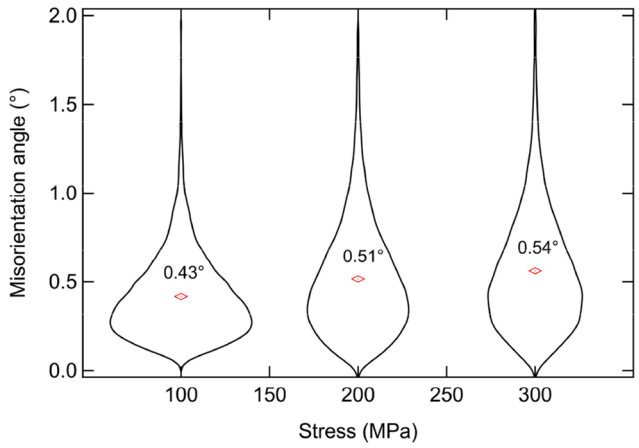

Fig. 5. A violin distribution plot of average misorientation angle of FeCo-2V against stress.

(108.89 A m^{-1}).

The variation of core loss with temperature is shown in Fig. 7. Core loss consistently decreased with increasing temperature. This pattern was observed uniformly across all tested frequencies, from 60 Hz to 800 Hz, indicating that thermal effects consistently reduce energy losses in the material. The decrease in core loss corresponds with the results shown in the hysteresis loops (Fig. 6), where the loop area became smaller at higher temperatures. Since the area of the hysteresis loop reflects the overall energy dissipated per cycle, its reduction at elevated temperatures directly supports the observed decrease in total core loss.

3.7. Loss – separation analysis of elevated temperature data

To investigate the reduction in total core loss with increasing temperature, a loss-separation analysis was conducted using Eq. 3. As with the data acquired under applied stress, each dataset were plotted as $\frac{P_{total}}{f}$ against $f^{1/2}$. A quadratic fit was then applied to each plot, yielding three coefficients: k_0, k_1 and k_2. An example fit is shown in Fig. 8.

The hysteresis loss coefficient (k_h) and eddy current loss coefficient (k_{ed}) were extracted from the quadratic fitting coefficients (k_0 and k_2) and plotted against temperature, as shown in Fig. 9a and 9b. Fig. 9a reveals a modest decrease in the hysteresis loss coefficient with increasing temperature, indicating a reduction in hysteresis loss at higher temperatures. Similarly, Fig. 9b shows a significant decrease in the eddy current loss coefficient with increasing temperature. This reduction contributes to the overall decline in eddy current loss at higher temperatures, further supporting the observed decrease in core loss.

3.8. Resistivity Measurement

The resistivity of FeCo-2V measured across three distinct strips over a temperature range of -40 °C to 170 °C revealed a clear increase in resistivity with rising temperature, as illustrated in Fig. 10. At -40 °C, the average resistivity of the FeCo-2V sample was measured to be approximately 0.42 μΩ m and reached 0.45 μΩ m at 170 °C. This trend continued uniformly across all three strips, demonstrating the reproducibility of the measurements.

4. Discussion

4.1. Effect of applied stress

The observed stress-dependent magnetic behaviour can be explained through magnetoelastic energy. When mechanical stress is applied to a magnetic material, the total anisotropy energy must account for stress-induced contributions. As detailed in previous studies [11,32,33], the magnetostriction and applied stress terms within the crystal anisotropy energy are collectively defined as magnetoelastic energy (E_{me}) and may be described by the equation.

$$E_{me} = \frac{3}{2}\lambda_s \sigma \sin^2\theta \tag{7}$$

where θ is the angle between the magnetisation and axis of the applied stress. The magnetisation behaviour under stress depends on the sign of magnetostriction (λ_s) and stress (σ).

To explain the behaviour of coercivity and core loss under compressive and tensile stresses, the response is divided into three parts: 1) degradation of magnetic properties under compressive stress, 2) initial improvement in magnetic properties at under moderate tensile stress, and 3) degradation of magnetic properties at high tensile stress.

1) Degradation of magnetic properties under compressive stress

The linear-shaped hysteresis loops observed under compressive stress (Fig. 1a) reveal magnetisation occurring along a hard axis. In

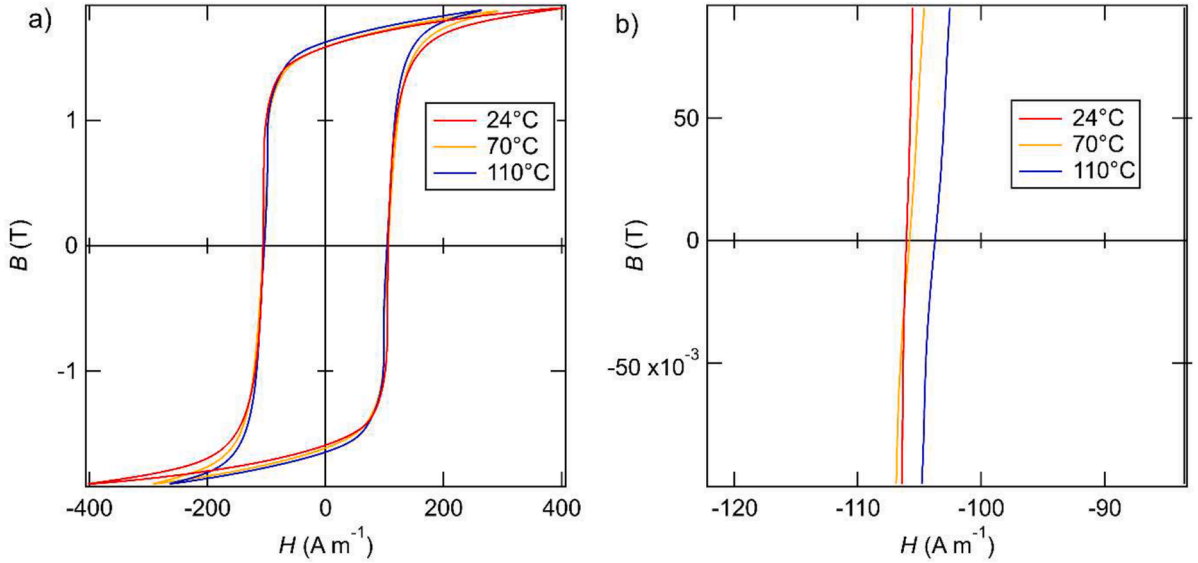

Fig. 6. Hysteresis curves measured at 100 Hz at different temperatures a) Full hysteresis loop b) Magnified part of hysteresis loop.

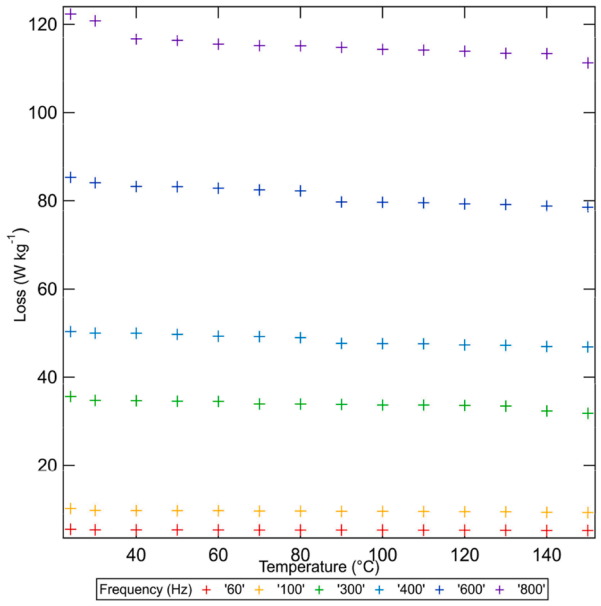

Fig. 7. A plot of core loss against temperature at different frequencies.

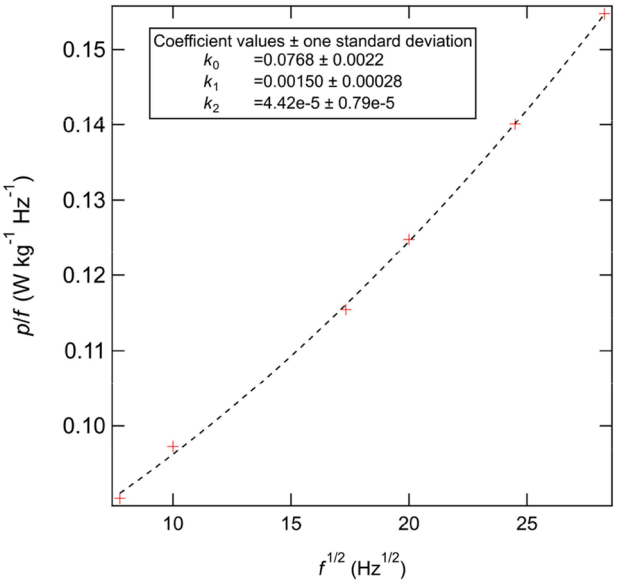

Fig. 8. Example of Loss separation analysis plot of sample at 30 °C and B = 2 T.

FeCo-2V, which exhibits positive magnetostriction ($\lambda_s > 0$), compressive stress (-σ) creates energetically unfavourable conditions for domains aligned parallel to the stress axis. As illustrated in Figs. 11b to 11c, domain walls preferentially eliminate these high magnetoelastic energy domains, leaving behind domains magnetised perpendicular to the stress direction. This domain elimination process follows directly from the magnetoelastic energy relationship (Eq. 7). Subsequent alignment with the applied magnetic field requires both domain growth and rotation (Fig. 11c to 11d), explaining the observed increases in coercivity and core losses at compressive stresses of -10 and -50 MPa.

These findings agree well with previous studies on various soft magnetic materials. Iordache and Hug [10] and Lahyaoui et al. [11] reported similar compression-induced magnetic hardening in non-oriented Si-Fe steels, while Miyagi et al. [12] observed comparable effects in electrical steels. Interestingly, Gorkunov et al. [13] demonstrated that tensile stress could produce equivalent degradation in 09G2S pipe steel, where the negative sign of $\lambda_s\sigma$ creates similar energetic conditions to compressive stress in positive-magnetostriction materials.

The agreement between the results of the present work and previous studies suggests that the fundamental mechanism of stress-induced magnetic anisotropy is broadly applicable across material types. However, the magnitude of the effect shows material dependence, with FeCo-2V exhibiting more pronounced changes than Si-Fe steels at equivalent stress levels. This difference likely comes from FeCo-2V's higher magnetostriction constant, which amplifies the magnetoelastic energy contribution [34].

2) Initial improvement in magnetic properties at under moderate tensile stress.

The square-shaped hysteresis loops observed during tensile loading (Fig. 1b and c) demonstrate different magnetic behaviour compared to compression. This distinct loop morphology indicates easy-axis magnetisation, with the stress axis becoming energetically favourable for domain alignment. In the low-stress regime (0 – ~ 100 MPa), a reduction in coercivity occurs along with a decrease in core losses, corresponding to decreasing hysteresis loop areas.

The underlying mechanism involves stress-assisted domain reorganisation (Figs. 11f to 11g), where tensile stress ($+\sigma$) and positive-magnetostriction ($\lambda_s > 0$) induce an elimination of domains oriented perpendicular to the loading direction. This is due to those domains having higher magnetoelastic energy than domains oriented parallel to the loading direction, according to Eq. 7. Subsequent magnetisation (Figs. 11g to 11h) proceeds primarily through energetically favourable domain growth rather than the combined growth and rotation mechanism required under compression. This simpler process reduces the energy required for magnetisation, explaining the improved soft magnetic properties.

These findings align with previous studies on similar systems. Turgut et al. [9] reported stress-induced improvements in FeCo alloys, with coercivity and power loss being reduced under moderate tension. Iordache and Hug [10] observed similar behaviour in FeCo-2V, while Lahyaoui et al. [11] documented similar enhancements in Si-Fe steels. The consistent observation of these effects across different materials (all with $\lambda_s\sigma > 0$) again supports the nature of this stress assisted magnetisation mechanism.

However, the stress thresholds for optimal magnetic enhancement vary significantly between materials. In the present study, FeCo-2V exhibited peak improvement at approximately 100 MPa, whereas the alloys investigated by Turgut et al. [9] and Thomas [35] showed optimal performance at lower stress levels of 50–60 MPa. These differences likely arise from variations in microstructure and grain size. Processing methods such as mechanical and magnetic annealing can result in different grain sizes in FeCo-2V, which, in turn, influence its magnetic properties [7,36]. Another contributing factor is the magnetostriction constant (λ_s); materials with higher λ_s values generally exhibit greater sensitivity to applied stress.

3) Degradation of magnetic properties after being subjected to a further increase in tensile stress.

Beyond ~ 100 MPa tensile stress, the magnetic properties of FeCo-2V exhibited significant degradation, marked by an increase in coercivity core losses. This reversal of the initial improvement correlates directly with the onset of micro-yielding, as evidenced by multiple experimental results.

The loss separation analysis revealed an increase in the hysteresis loss coefficient (k_h) between 100-300 MPa, strongly suggesting magnetic domain wall pinning effects. This interpretation is consistent with classical models where dislocations act as pinning sites for domain walls [37], creating energy barriers that impede magnetisation processes. The rise in k_h values indicates that dislocation density increases with applied stress, in agreement with previous reports on FeCo alloys [9,10].

Complementary EBSD analysis provided microstructural support for

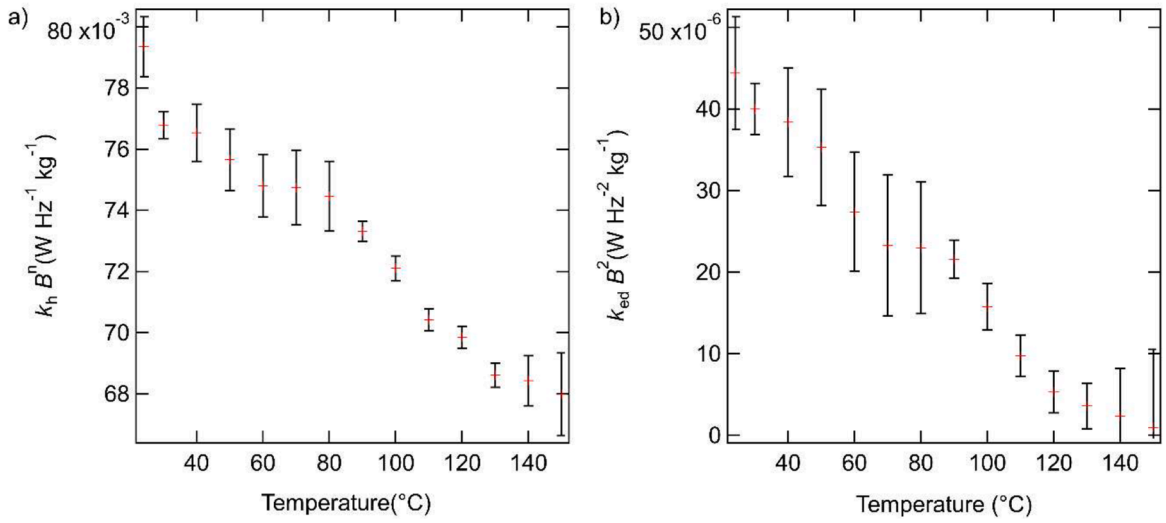

Fig. 9. A plot of a) hysteresis loss and b) eddy current loss coefficients against temperature.

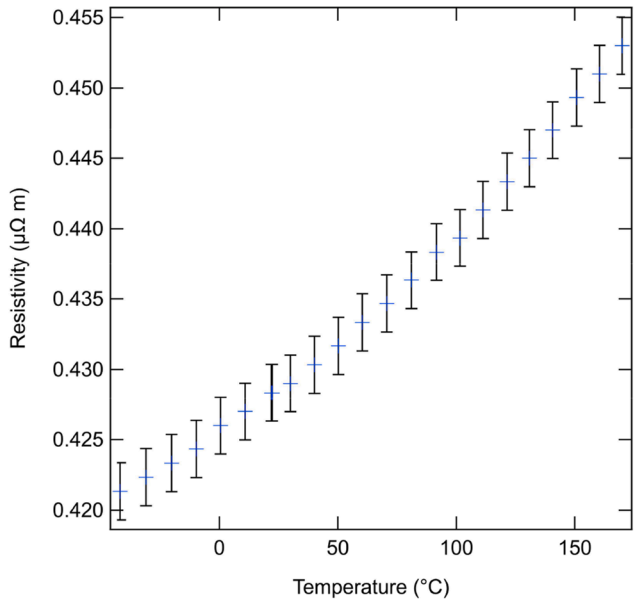

Fig. 10. A plot of average resistivity of FeCo-2V samples against temperature.

these findings. The measured increase in KAM angles from 0.43° (100 MPa) to 0.54° (300 MPa) over this stress range directly demonstrates enhanced localised deformation, characteristic of rising dislocation densities. These microstructural changes correlate well with the observed magnetic property degradation, as dislocations increasingly hinder domain wall motion [21,38–41].

The observed increase in KAM with stress provides microstructural evidence of micro-yielding, where localised plastic deformation initiates even though the bulk material remains below its macroscopic yield strength. Micro-yielding is characterised by the creation and multiplication of dislocations in specific grains or grain clusters subjected to stress concentrations. These dislocations generate strain fields that interact strongly with magnetic domain walls.

From a magnetic standpoint, each dislocation acts as a pinning site, increasing the energy barrier that domain walls must overcome during magnetisation reversal [40,41]. As the density of these pinning sites rises with micro-yielding, the domain walls require progressively higher field strengths to move, resulting in increased coercivity and larger hysteresis losses. This mechanism explains why magnetic degradation emerges beyond ~100 MPa despite the material still being nominally in the elastic regime. The combined increase in KAM values, hysteresis loss coefficient, and coercivity therefore provides a consistent picture: micro-yielding produces dislocation structures that impede domain wall motion, leading to the observed deterioration in magnetic performance at high tensile stresses.

4.2. *Effect of elevated temperature*

The reduction in core loss observed in the FeCo-2V alloy with increasing temperature can be attributed to two primary mechanisms. First, temperature affects hysteresis loss by reducing magnetic anisotropy and facilitating domain wall motion. Second, temperature influences eddy current loss, primarily through changes in the resistivity of FeCo-2V.

The reduction in hysteresis loss observed in the FeCo-2V alloy with increasing temperature can be attributed to changes in the material's magnetic domain behaviour. Hysteresis loss and coercivity are closely linked to the alignment and motion of magnetic domains in response to an external magnetic field. These processes depend on the ease with which domain walls can reorient and move, which is influenced by the magnetocrystalline anisotropy and microstructural defects [15].

Magnetocrystalline anisotropy, governed by the anisotropy constant, plays a critical role in determining the material's magnetic behaviour. The domain wall energy is directly proportional to the square root of the anisotropy constant. This relationship indicates that materials with higher anisotropy constants require more energy to reorient magnetic domains, leading to increased coercivity and hysteresis loss [42,43].

The results of this study, as shown in Fig. 9a, demonstrate a reduction in the hysteresis loss coefficient with increasing temperature, indicating easier domain wall motion at higher temperatures. This trend aligns with previous studies by Vértesy [44], De Campos [45] and Duranka et al. [46], which reported a correlation between reduced anisotropy energy and lower coercivity and hysteresis loss. Within the temperature range of this experiment, factors such as impurity concentration and grain structure remained constant, ruling out their influence on the observed changes [6,7]. Instead, the decrease in anisotropy energy due to thermal agitation is likely the primary cause of the reduction in coercivity and hysteresis loss. At elevated temperatures, thermal energy disrupts the alignment preferences of magnetic moments within the crystal lattice. This thermal agitation competes with the intrinsic directional preferences of the crystal structure, weakening the material's ability to maintain a specific magnetic orientation. As a result, anisotropy energy decreases, reducing the energy required for domain wall

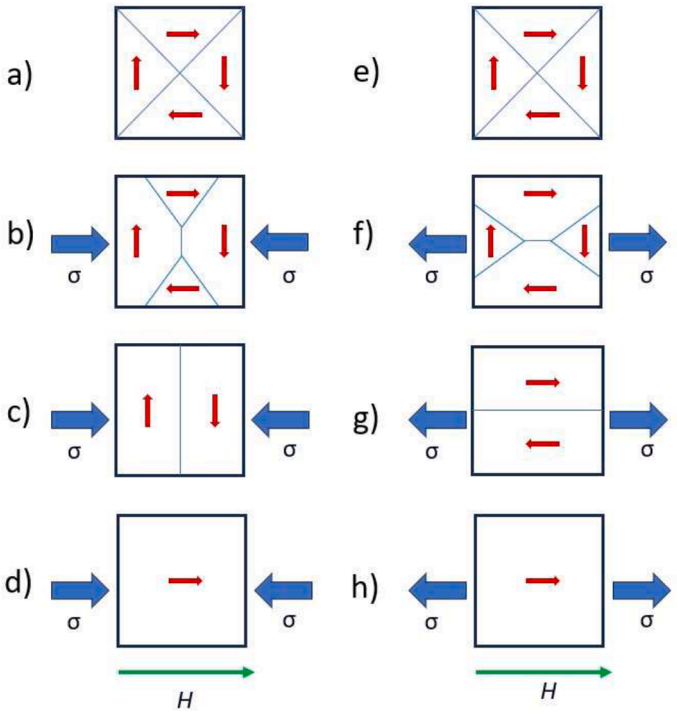

Fig. 11. Schematic illustration of domain magnetisation processes in a material with positive magnetostriction under applied stress. Panels (a–d) show the effect of compressive stress (-σ), while panels (e–h) show the effect of tensile stress (+σ). Adapted from [32].

motion and magnetisation. This effect leads to a decrease in both coercivity and hysteresis loss, consistent with the observed results [2,40]. These findings align with the behaviour of other soft magnetic materials, where thermal energy lowers energy barriers for domain wall motion, facilitating easier magnetisation and reducing energy losses.

The relationship between temperature and hysteresis loss has been further supported by studies such as those by Ferro et al. [2,47], who reported that the decrease in hysteresis loss with increasing temperature is primarily driven by the reduction in crystalline anisotropy energy and the anisotropy constant. As temperature rises, thermal energy disrupts magnetic domain alignment, lowering the energy barriers for domain wall motion. This results in easier magnetisation processes, narrower hysteresis loops, and reduced hysteresis losses. Experimental results on directional Fe-Si confirm that the temperature dependence of hysteresis loss is closely tied to the material's intrinsic magnetic properties, particularly its anisotropy energy. These findings are consistent with the results of this study and can be used to explain the observed reduction in hysteresis loss in FeCo-2V.

The decrease in the eddy current loss coefficient (k_{ed}) observed in Fig. 9b, as temperature increased from 24 °C to 150 °C, and the corresponding increase in resistivity from -40 °C to 170 °C, shown in Fig. 10, can both be attributed to a reduction in the electron mean free path. According to the Drude model [48], electrical resistivity is inversely proportional to the mean free path, as shown in Eq. 8:

$$\rho = \frac{mv}{ne^2\lambda} \tag{8}$$

Where ρ is resistivity, m is electron mass, n is electron density, v is drift velocity or average electron velocity, e is electron charge, and λ is mean free path of electron.

Electrical resistivity depends on factors such as temperature and material purity. At low temperatures, impurity and defect scattering dominate, and because phonon activity is minimal, these static imperfections primarily determine the electron mean free path. As temperature increases, however, electron–phonon interactions become the major scattering mechanism. Enhanced atomic vibrations create additional dynamic obstacles for electron movement, causing more frequent collisions and shortening the mean free path. Although impurity scattering remains present at higher temperatures, its contribution becomes comparatively weaker than the rapidly increasing phonon scattering; nonetheless, defects, alloying elements, and interfacial irregularities still add to the overall resistivity by providing an elevated baseline, a behaviour also noted in recent studies [49]. These combined effects lead to the typical rise in resistivity observed in conductive and magnetic materials as temperature increases [50,51]. The observed resistivity increase in this study aligns with findings by Purewal et al. [50] and Anderson et al. [52], who reported similar trends in other magnetic materials. These studies also identified the reduction in electron mean free path as the primary mechanism behind the rise in resistivity at higher temperatures.

The increase in resistivity with temperature has a direct impact on eddy current losses as the eddy current loss coefficient (k_{ed}) is inversely proportional to resistivity. This relationship is consistent with the findings of Xue et al. [53], who demonstrated that eddy current losses decrease with rising temperature due to increased resistivity, which reduces the eddy current loss coefficient. Similarly, Foster [54] and Regnet et al. [55] observed that higher resistivity at elevated temperatures leads to a reduction in eddy current losses, as the increased scattering of electrons reduces the mean free path and limits the formation of eddy currents.

While the linear resistivity-temperature relationship shown in Fig. 10 would theoretically predict a decrease in k_{ed} following an inverse dependence on resistivity ($\frac{1}{\rho}$), the experimental results in Fig. 9b deviate slightly from this expected trend. This discrepancy can be attributed to secondary thermal effects, particularly dimensional changes caused by thermal expansion that slightly modify the thickness of the material. Regardless of the specific origin of this deviation, the dominant effect remains clear: increasing resistivity with temperature consistently reduces eddy current loss, thereby contributing to the overall decrease in total core loss as established in prior discussion.

Although this study separately examined the effects of mechanical stress and temperature on the magnetic properties of FeCo-2V, real

electrical machine components experience both influences simultaneously. The thermo-mechanical interaction may introduce non-linearities because stress tends to modify magnetoelastic anisotropy, while temperature reduces magnetocrystalline anisotropy and electrical conductivity. These competing mechanisms could act synergistically or antagonistically depending on operating conditions. Due to limitations in the current experimental setup, simultaneous application of controlled stress and temperature was not possible here, but incorporating combined thermo-mechanical testing would provide valuable insight and improve the predictive capability of magnetic material models under service-relevant conditions.

Furthermore, future work could significantly benefit from direct magnetic domain imaging. Techniques such as Magneto-Optic Kerr Effect (MOKE) microscopy or Lorentz TEM would enable real-time visualisation of stress-assisted domain alignment and the interaction between domain walls and stress-induced dislocation structures. Such measurements would provide complementary evidence to the macroscopic magnetic and microstructural results presented here and further validate the mechanisms proposed in this study.

5. Conclusion

The effects of applied stress and of temperature on the magnetic properties of the FeCo-2V alloy were investigated. The main factor contributing to the changes in magnetic properties under applied stress was identified as the magnetisation along the easy and hard axes, influenced by coupling between magnetostriction and applied stress. In the compressive stress region, hysteresis loops exhibited a linear shape. As compressive stresses increased, the loops expanded and rotated, signifying an increase in coercivity and hysteresis loss. This indicated that magnetisation occurred along the hard axis. Hysteresis loops under tensile stress displayed a square-like shape, signifying magnetisation along the easy axis. Initially, under tensile stress from 0 MPa to ~ 100 MPa, the hysteresis loop contracted, indicating an improvement in the coercivity and core loss. However, beyond a tensile stress of around 100 MPa, the hysteresis loop expanded, and coercivity and core loss increased. This degradation of magnetic properties arose from magnetic domain wall pining by an increase in dislocation density associated with micro-yielding.

Loss separation analyses indicated that the rise in core loss was primarily attributable to hysteresis loss. The coefficient of hysteresis loss was observed to increase with applied tensile stress, suggesting impeded domain wall motion and the degradation of magnetic properties. This rise in the hysteresis loss coefficient was attributed to an increase in dislocation density resulting from micro-yielding, a conclusion supported by an increase in KAM average misorientation angle with increased applied stress.

Measurements of the magnetic properties with temperature revealed a clear trend of decreasing core losses with increasing temperature, driven by reductions in both hysteresis and eddy current losses. The decrease in hysteresis loss is primarily attributed to thermally induced reductions in anisotropy energy. Elevated temperatures promote thermal agitation that lower the anisotropy energy. This facilitates easier domain wall motion, leading to a decrease in hysteresis loss.

In parallel, eddy current loss was also observed to diminish with rising temperature. This behaviour is linked to an increase in the electrical resistivity of the FeCo-2V alloy, which results from a reduced electron mean free path due to enhanced electron scattering at higher temperatures. As resistivity increases, the magnitude of induced eddy currents decreases, leading to a corresponding reduction in associated total energy losses.

Declaration of generative AI and AI-assisted technologies in the writing process

During the preparation of this work the authors used ChatGPT in order to improve grammar. After using this tool/service, the authors reviewed and edited the content as needed and take full responsibility for the content of the publication.

CRediT authorship contribution statement

Sirapob Toyting: Writing – original draft, Visualization, Project administration, Investigation, Formal analysis, Conceptualization. **Christopher W. Harrison:** Writing – review & editing, Supervision, Methodology, Investigation. **Alexis Lambourne:** Writing – review & editing, Resources, Funding acquisition. **Howard J. Stone:** Writing – review & editing, Supervision, Project administration, Funding acquisition, Conceptualization.

Declaration of competing interest

The authors declare the following financial interests/personal relationships which may be considered as potential competing interests: S. Toyting reports financial support was provided by Royal Thai Government Ministry of Science and Technology. S. Toyting reports financial support was provided by Rolls-Royce plc. If there are other authors, they declare that they have no known competing financial interests or personal relationships that could have appeared to influence the work reported in this paper.

Acknowledgements

This work was financially supported by Royal Thai government scholarship and Rolls-Royce plc.

Data availability

Data will be made available on request.

References

[1] D. Jiles, Soft Magnetic Materials. Introduction to Magnetism and Magnetic Materials, 3rd ed., CRC Press, Boca Raton, 2015, pp. 321–326.
[2] F. Fiorillo, Soft Magnetic Materials. Characterization and Measurement of Magnetic Materials, Elsevier, 2004, pp. 25–88, https://doi.org/10.1016/B978-012257251-7/50004-6.
[3] G. Herzer, Modern soft magnets: Amorphous and nanocrystalline materials, Acta Mater. 61 (3) (Feb. 2013) 718–734, https://doi.org/10.1016/j.actamat.2012.10.040.
[4] S. Tumanski, *Handbook of Magnetic Measurements*, 0 ed, CRC Press, 2016, https://doi.org/10.1201/b10979.
[5] R. Hilzinger, W. Rodewald, Cobalt-iron alloys. *Magnetic materials: fundamentals, products, properties, and applications*, Erlangen, Hanau, Germany, Publicis; VAC, VACUUMSCHMELZE Erlangen, Hanau, Germany, 2013, pp. 226–232.
[6] R.S. Sundar, S.C. Deevi, Soft magnetic FeCo alloys: alloy development, processing, and properties, Int. Mater. Rev. 50 (3) (June 2005) 157–192, https://doi.org/10.1179/174328005X14339.
[7] T. Sourmail, Near equiatomic FeCo alloys: Constitution, mechanical and magnetic properties, Prog. Mater. Sci. 50 (7) (Sept. 2005) 816–880, https://doi.org/10.1016/j.pmatsci.2005.04.001.
[8] J. H. White and C. V. Wahl, "Workable magnetic compositions containing principally iron and cobalt," 1862559, June 14, 1932.
[9] Z. Turgut, M.Q. Huang, J.C. Horwath, R. Hinde, J. Kubicki, R.T. Fingers, Effect of Tensile Stress and Texture on Magnetic Properties of FeCo Laminates, IEEE Trans. Magn. 40 (4) (July 2004) 2742–2744, https://doi.org/10.1109/TMAG.2004.832119.
[10] V.E. Iordache, E. Hug, Effect of Mechanical Strains on the Magnetic Properties of Electrical Steels, J. Optoelectron. Adv. Mater. 6 (4) (Dec. 2004) 1297–1303.
[11] O. Lahyaoui, V. Lanfranchi, N. Buiron, F. Martin, U. Aydin, A. Belahcen, Effect of mechanical stress on magnetization and magnetostriction strain behavior of non-oriented Si-Fe steels at different directions and under pseudo-DC conditions, Int. J. Appl. Electromagn. Mech. 60 (2) (June 2019) 299–312, https://doi.org/10.3233/JAE-180106.
[12] D. Miyagi, K. Miki, M. Nakano, N. Takahashi, Influence of Compressive Stress on Magnetic Properties of Laminated Electrical Steel Sheets, IEEE Trans. Magn. 46 (2) (2010) 318–321, https://doi.org/10.1109/TMAG.2009.2033550.
[13] E.S. Gorkunov, S.M. Zadvorkin, A.N. Mushnikov, S.V. Smirnov, E.I. Yakushenko, Effect of mechanical stresses on the magnetic characteristics of pipe steel, J. Appl. Mech. Tech. Phys. 55 (3) (May 2014) 530–538, https://doi.org/10.1134/S002189441403016X.

[14] L. Ferraris, F. Franchini, E. Pošković, M.Actis Grande, R. Bidulský, Effect of the Temperature on the Magnetic and Energetic Properties of Soft Magnetic Composite Materials, Energies 14 (15) (July 2021) 4400, https://doi.org/10.3390/en14154400.
[15] H. C. de Groh III, S. M. Geng, J. M. Niedra, and R. R. Hofer, "Magnetic properties of Fe-49Co-2V alloy and pure Fe at room and elevated temperatures," Apr. 2018.
[16] Y. Li, C. Jin, M. Yang, S. Mu, C. Zhang, Magnetic property measurement and analysis of high-frequency soft magnetic materials under non-sinusoidal excitation considering temperature effect, AIP Adv 13 (3) (Mar. 2023) 035031, https://doi.org/10.1063/9.0000469.
[17] C.-H. Shang, R. C. Cammarata, T. P. Weihs, and C. L. Chien, "Microstructure and Hall–Petch behavior of Fe–Co-based Hiperco© alloys)".
[18] VACOFLUX 50, VACUUMSCHMELZE GmbH & Co [Online]. Available, https://vacuumschmelze.com/03_Documents/Brochures/Flyer%20VACOFLUX%2050.pdf, July 2022.
[19] T. Sourmail, Evolution of strength and coercivity during annealing of FeCo based alloys, Scr. Mater. 51 (6) (Sept. 2004) 589–591, https://doi.org/10.1016/j.scriptamat.2004.05.028.
[20] Z. Li, Z. Chen, J.T. Oh, V. Gill, A. Lambourne, Improving the mechanical and magnetic properties of equiatomic FeCo-2V alloy through mild magnetic field annealing, Metall. Mater. Trans. A 55 (10) (Oct. 2024) 4061–4071, https://doi.org/10.1007/s11661-024-07527-0.
[21] A. Daem, P. Sergeant, L. Dupré, S. Chaudhuri, V. Bliznuk, L. Kestens, Magnetic properties of silicon steel after plastic deformation, Materials 13 (19) (Sept. 2020) 4361, https://doi.org/10.3390/ma13194361.
[22] S.G. Ghalamestani, T. Hilgert, S. Billiet, L. Vandevelde, J.A. Melkebeek, J.J. J. Dirckx, Measurement of magnetostriction using dual laser heterodyne interferometers: experimental challenges and preliminary results [Online]. Available: https://api.semanticscholar.org/CorpusID:67840177, 2009.
[23] IEC 60404-3:2022, Magnetic materials - Part 3: Methods of measurement of the magnetic properties of electrical steel strip and sheet by means of a single sheet tester, Nov. 08, 2022.
[24] *IEC 60404-4:1995*, Magnetic materials - Part 4: Methods of measurement of d.c. magnetic properties of iron and steel, Feb. 15, 1995.
[25] P. Mallett, P. Anderson, C. Harrison, Measuring the coupled effect of heat and stress on the magnetic properties of electrical steel, in: Proceedings of the Cardiff University Engineering Research Conference 2023, Cardiff University Press, May 2024, pp. 145–147, https://doi.org/10.18573/conf1.ag.
[26] P. Anderson, Measurement techniques for the assessment of materials under complex magnetising conditions, Przeglad Elektrotechniczny 87 (2011) 61–64.
[27] G. Bertotti, General properties of power losses in soft ferromagnetic materials, IEEE Trans. Magn. 24 (1) (Jan. 1988) 621–630, https://doi.org/10.1109/20.43994.
[28] K. Yamazaki, N. Fukushima, Iron-loss modeling for rotating machines: comparison between Bertotti's three-term expression and 3-D eddy-current analysis, IEEE Trans. Magn. 46 (8) (Aug. 2010) 3121–3124, https://doi.org/10.1109/TMAG.2010.2044384.
[29] T. Wang, J. Yuan, Improvement on loss separation method for core loss calculation under high-frequency sinusoidal and nonsinusoidal excitation, IEEE Trans. Magn. 58 (8) (Aug. 2022) 1–9, https://doi.org/10.1109/TMAG.2022.3187206.
[30] BS EN 6404-13:1996, Magnetic materials - Methods of measurement of density, resistivity and stacking factor of electrical steel sheet and strip, May 15, 1996.
[31] W. Pieper, J. Gerster, Total power loss density in a soft magnetic 49% Co–49% Fe–2% V-alloy, J. Appl. Phys. 109 (7) (Apr. 2011) 07A312, https://doi.org/10.1063/1.3537956.
[32] B.D. Cullity, C.D. Graham, Magnetostriction and the Effects of Stress. Introduction to Magnetic Materials, John Wiley & Sons, Ltd, 2008, pp. 241–273, https://doi.org/10.1002/9780470386323.ch8.
[33] T.W. Krause, L. Clapham, A. Pattantyus, D.L. Atherton, Investigation of the stress-dependent magnetic easy axis in steel using magnetic Barkhausen noise, J. Appl. Phys. 79 (8) (Apr. 1996) 4242–4252, https://doi.org/10.1063/1.361878.
[34] R. Hilzinger, W. Rodewald, Properties and characteristic curves of soft magnetic materials and ductile permanent magnets. *Magnetic materials: fundamentals, products, properties, and applications*, Erlangen, Hanau, Germany, Publicis; VAC, VACUUMSCHMELZE, Erlangen, Hanau, Germany, 2013, pp. 305–399.
[35] B. Thomas, A quantitative assessment of the change in magnetic properties of Co-Fe-V alloy when subjected to flux and stress conditions similar to those encountered in an aircraft generator, IEEE Trans. Magn. 16 (5) (Sept. 1980) 1299–1309, https://doi.org/10.1109/TMAG.1980.1060841.
[36] Z. Li, et al., Mechanical properties and fractographic analyses of FeCo-2V alloy heat-treated around order-disorder transition temperature, J. Mater. Res. Technol. 22 (Jan. 2023) 3302–3310, https://doi.org/10.1016/j.jmrt.2022.12.142.
[37] " in "Ferromagnetism, Introduction to Magnetic Materials, John Wiley & Sons, Ltd, 2008, pp. 115–149, https://doi.org/10.1002/9780470386323.ch4.
[38] N.A. Spaldin, Ferromagnetic domains. Magnetic Materials: Fundamentals and Applications, Cambridge University Press, 2010, pp. 79–95.
[39] B.D. Cullity, C.D. Graham, Introduction to Magnetic Materials (2008), https://doi.org/10.1002/9780470386323.
[40] R. Hilzinger, W. Rodewald, Magnetization process. Magnetic materials: fundamentals, products, properties, and applications, Publicis; VAC, VACUUMSCHMELZE Erlangen, Hanau, Germany, Erlangen, Hanau, Germany, 2013, pp. 58–72.
[41] O. Hubert, E. Hug, I. Guillot, M. Clavel, Effect of internal stresses and dislocation features on the magnetic properties of soft ferromagnetic materials, J. Phys. IV 08 (PR2) (June 1998), https://doi.org/10.1051/jp4:19982119 pp. Pr2-515-Pr2-518.
[42] R. Hilzinger, W. Rodewald, Magnetic domains and process of magnetization. Magnetic materials: fundamentals, products, properties, and applications, Publicis; VAC, VACUUMSCHMELZE Erlangen, Hanau, Germany, Erlangen, Hanau, Germany, 2013, pp. 45–72.
[43] Domains and the Magnetization Process, Introduction to Magnetic Materials, John Wiley & Sons, Ltd, 2008, pp. 275–333, https://doi.org/10.1002/9780470386323.ch9.
[44] G. Vértesy, Temperature Dependence of Coercivity of Some Soft Magnetic Materials, in: G.C. Hadjipanayis (Ed.), Magnetic Hysteresis in Novel Magnetic Materials, Springer Netherlands, Dordrecht, 1997, pp. 737–741, https://doi.org/10.1007/978-94-011-5478-9_79.
[45] M.F. De Campos, Coercivity mechanism in hard and soft sintered magnetic materials, Mater. Sci. Forum 802 (Dec. 2014) 563–568, https://doi.org/10.4028/www.scientific.net/MSF.802.563.
[46] P. Duranka, J. Onufer, J. Ziman, Effect of temperature on domain wall dynamics in magnetic microwire, presented at the, in: 1st International Conference on Radiations and Applications (ICRA-2017), Algiers, Algeria, 2018, https://doi.org/10.1063/1.5048860.
[47] A. Ferro, G. Montalenti, G. Soardo, Temperature dependence of power loss anomalies in directional FeSi 3%, IEEE Trans. Magn. 12 (6) (Nov. 1976) 870–872, https://doi.org/10.1109/TMAG.1976.1059112.
[48] R.E. Hummel, Electrical conduction in metals and alloys. Electronic Properties of Materials, Springer New York, New York, NY, 2011, pp. 79–114, https://doi.org/10.1007/978-1-4419-8164-6_7.
[49] R. Wang, et al., FeSi@BN soft magnetic composites inspired by fried glutinous rice balls: A core–shell design for enhanced magnetic and thermal performance in high-frequency power applications, Chem. Eng. J. 515 (July 2025) 163501, https://doi.org/10.1016/j.cej.2025.163501.
[50] M.S. Purewal, B.H. Hong, A. Ravi, B. Chandra, J. Hone, P. Kim, Scaling of Resistance and Electron Mean Free Path of Single-Walled Carbon Nanotubes, Phys. Rev. Lett. 98 (18) (May 2007) 186808, https://doi.org/10.1103/PhysRevLett.98.186808.
[51] J.C. Mauro, Thermal and electrical conductivities. Materials Kinetics, Elsevier, 2021, pp. 501–511, https://doi.org/10.1016/B978-0-12-823907-0.00010-8.
[52] P. Anderson, D.Rhys Jones, J. Hall, Measurement of resistivity of soft magnetic laminations at elevated temperatures, J. Magn. Magn. Mater. 304 (2) (Sept. 2006) e546–e548, https://doi.org/10.1016/j.jmmm.2006.02.151.
[53] S. Xue, J. Feng, S. Guo, J. Peng, W.Q. Chu, Z.Q. Zhu, A new iron loss model for temperature dependencies of hysteresis and eddy current losses in electrical machines, IEEE Trans. Magn. 54 (1) (Jan. 2018) 1–10, https://doi.org/10.1109/TMAG.2017.2755593.
[54] K. Foster, Temperature dependence of loss separation measurements for oriented silicon steels, IEEE Trans. Magn. 22 (1) (Jan. 1986) 49–53, https://doi.org/10.1109/TMAG.1986.1064276.
[55] M. Regnet, T. Schäufele, A. Dietz, B. Löhlein, Temperature influence on core losses and magnetization demand of electrical steel sheets using adapted Epstein frame and ring probe, in: 2023 13th International Electric Drives Production Conference (EDPC), IEEE, Regensburg, Germany, Nov. 2023, pp. 1–7, https://doi.org/10.1109/EDPC60603.2023.10372149.